Crystal structure and electrical properties of textured Ba2Bi4Ti5O18 ceramics

REPOSITORY RECORD

Crystal structure and electrical properties of textured $Ba_2Bi_4Ti_5O_{18}$ ceramics

Jun Cao,[1] Vladimir Koval,[2] Hangfeng Zhang,[1] Yunyin Lin,[1] Jiyue Wu,[1] Nan Meng,[1]

Yan Li,[4] Zheng Li,[1*] Hongtao Zhang,[3*] Haixue Yan[1]

[1] School of Engineering and Materials Science, Queen Mary University of London, Mile End Road,

London, E1 4NS, United Kingdom

[2] Institute of Materials Research, Slovak Academy of Sciences, Watsonova 47, 04001 Kosice,

Slovakia

[3] Department of Materials, Loughborough University, Leicestershire, LE11 3TU, United Kingdom

[4] Gemmological Institute, China University of Geosciences, Wuhan, 430074, PR China

*Corresponding authors

H. Zhang's email: h.zhang3@lboro.ac.uk

Z. Li's email: zheng.li@qmul.ac.uk

Abstract

Highly textured $Ba_2Bi_4Ti_5O_{18}$ ceramic was prepared by spark plasma sintering (SPS). X-ray diffraction of the ceramics revealed the coexistence of a major ferroelectric phase (Space group, SG: *B2cb*) and a minor paraelectric phase (SG: *I4/mmm*) at room temperature. A diffused phase transition was observed at around 240 °C. The evolution of the switching current peaks in the electric current *vs*. electric field (*I-E*) loops with increasing temperature was interpreted by the structural changes and temperature dependent polarisation reversal processes. The slim polarisation *vs*. electric field (*P-E*) loops, the extra switching current peaks in the *I-E* loops and the non-zero piezoelectric d_{33} coefficient indicate that $Ba_2Bi_4Ti_5O_{18}$ is a relaxor ferroelectric material. The recoverable energy density (0.41 ± 0.01 J/cm^3) of $Ba_2Bi_4Ti_5O_{18}$ ceramics in the perpendicular direction to the SPS pressing direction is close to that of $Pb(Mg_{1/3}Nb_{2/3})O_3$-based ceramics. The obtained results suggest $Ba_2Bi_4Ti_5O_{18}$ ceramics might be promising for energy storage applications.

Keywords: $Ba_2Bi_4Ti_5O_{18}$, texture, relaxor ferroelectrics, bismuth layer-structured ferroelectrics, energy storage.

Introduction

Compared to normal ferroelectrics, relaxor ferroelectrics (RFEs) are more attractive for energy storage applications due to their high energy density related to a low remnant polarization and a high saturated polarisation [1,2]. RFEs exhibit a broad, frequency-dependent, dielectric anomaly at the temperature (T_m) of the maximum of the relative dielectric permittivity. Most of the current research on RFEs is focused on lead-based complex perovskites, such as $Pb(Mg_{1/3}Nb_{2/3})O_3$-$PbTiO_3$, $Pb(Mg_{1/3}Nb_{2/3})O_3$-$Pb(Zr,Ti)O_3$ and $Pb(Zn_{1/3}Nb_{2/3})O_3$-$PbTiO_3$ [3,4]. However, relatively low T_m or Curie point (T_c) of these relaxor systems restrict their high-temperature applications. Therefore, there is a great effort in developing new lead-free RFEs materials with higher ferroelectric phase transition temperatures for energy storage applications. Bismuth layer-structured ferroelectrics (BLSFs) are well known lead-free materials for high-temperature piezoelectric applications due to their high T_c and large polarisation and fatigue-free behaviour [5-9]. BLSFs with the general formula $(Bi_2O_2)^{2+}(A_{m-1}B_mO_{3m+1})^{2-}$ can be described as the regular stacking of $[Bi_2O_2]^{2+}$ layers and pseudo-perovskite $(A_{m-1}B_mO_{3m+1})^2$ slabs, where m denotes the number of sheets of corner-sharing BO_6 octahedra. The 12-coordinated A-site can be occupied by mono-, di-, or trivalent metallic cations, while the octahedral-coordinated B-sites are entered by tetra-, penta-, or hexavalent metallic cations [10,11]. Within the BLSFs family, only a limited number of compounds, such as $BaBi_2Nb_2O_9$, $BaBi_2Ta_2O_9$, and $BaBi_4Ti_4O_{15}$, shows the relaxor ferroelectric characteristics [12-14]. The RFE behavior in these systems is attributed to the positional static disorder between Bi^{3+} and Ba^{2+} ions driven by a fluctuation in chemical composition [15]. However, on contrary to the above mentioned lead-based RFEs, an understanding on relaxor behavior of BLSFs and literature about possible applications of these materials in energy storage are extremely limited.

Ba$_2$Bi$_4$Ti$_5$O$_{18}$ (B2BT) belongs to the family of BLSFs that exhibit relaxor characteristics [10,11]. The Ba and Bi ions occupy the A-sites and the Ti ions enter the B-sites of the pseudo-perovskite blocks (A$_{m-1}$B$_m$O$_{3m+1}$)$^{2-}$. The synthesis and ferroelectric properties of B2BT were first reported by Aurivillius and Subbarao in 1962 [16,17]. However, the existence of single phase B2BT is still disputable. While Subbarao reported a mixture of a four-layer oxide BaBi$_4$Ti$_4$O$_{15}$ and BaTiO$_3$ in the B2BT ceramics synthesized via solid state reaction [17], Aurivillius found only a single tetragonal phase [space group (SG): *I4/mmm*] in B2BT single crystal. The existence of an exclusive non-polar structure in the B2BT single crystal precludes the observation of the ferroelectric hysteresis loop, such as reported in Ref. 16. Moreover, Aurivillius observed a maximum of the dielectric permittivity at 329 °C, suggesting the ferroelectric-to-paraelectric phase transition [16]. Irie *et al*. reported an orthorhombic *B2ab* symmetry of the B2BT single crystal [10,11]. They measured the polarisation *vs*. electric field (*P-E*) loops of the crystal in different directions and found that the remnant polarisation (*P$_r$*) shows non-zero values along both the *a*-axis (or *b*-axis) and the *c*-axis. On the other hand, *P$_r$* (~ 8.5 mC/m^2) measured along the *c*-axis does not comply with the symmetry conditions of the space group *B2ab*. In addition, the frequency dependence of the maximum relative dielectric permittivity ($\varepsilon_{r\,\text{max}}$) observed along both the ***a***- or ***b***-axis and the ***c***-axis suggests RFE behaviour. Based on high-resolution powder neutron diffraction data, Ismunandar demonstrated that the crystal structure of B2BT is orthorhombic with space group *B2eb* (an alternative setting of *B2ab*) [18]. On contrary, using high-resolution powder neutron diffraction, Lightfoot *et al*. showed that B2BT adopts a tetragonal *I4/mmm* structure at room temperature [19]. Synchrotron x-ray diffraction study by Fuentes *et al*. confirmed the tetragonal (*I4/mmm*) structure of the B2BT ceramics [20]. Hou *et al*. observed a very broad frequency-independent dielectric anomaly in B2BT ceramics at about 330 °C from 10 kHz to 1 MHz [21]. No piezoelectric response was detected after poling the ceramics [21]. Dubey *et al*. synthesized the B2BT

4

powder by a solution combustion route [22]. The sintered B2BT had an orthorhombic symmetry (*B2cb*) and exhibited a diffuse phase transition at about 350 °C. The transition temperature of the B2BT ceramic was slightly sensitive to the measuring frequency. Therefore, it is clear that the current understanding of both the crystal structure and electrical properties of B2BT ceramics is inconsistent with many controversial issues. Furthermore, only a very little is known about energy storage capability of relaxor-type BLSFs.

Single crystals are considered the most suitable materials for studying the RFE behavior. They enable to evaluate variations in the electrical response of a relaxor with respect to the different crystal axes [23]. However, fabrication of single crystals of BLSFs is difficult because of the complex oxide structure. The grains in sintered BLSFs ceramics are randomly orientated so that the measured properties correspond to the average value over each direction and grain. Highly textured ceramics with oriented grains mimic a pseudo-single crystal structure and exhibit the enhanced electrical properties [7,24]. The BLSF ceramics with a preferential orientation of grains have been produced by spark plasma sintering (SPS) technique [7,24,25].

In this work, we prepared the grain-oriented B2BT ceramics, as a potential candidate for energy storage applications, by SPS technique. The crystal structure, dielectric, ferroelectric, and piezoelectric properties of B2BT ceramics were systemically investigated in the parallel and perpendicular direction to the direction of the SPS pressing. This is, to our best knowledge, the first report about the processing, microstructure and electrical properties of the textured B2BT ceramics with a great capability for high-density energy storage.

Materials and methods

Sample preparation: The $Ba_2Bi_4Ti_5O_{18}$ powder was prepared by the conventional solid-state reaction route. Bi_2O_3 (99.9%, Sigma-Aldrich), TiO_2 (99.8%, Sigma-Aldrich) and $BaCO_3$ (99.8%, Sigma-Aldrich) were used as starting materials. The stoichiometric mixture of raw materials was thoroughly mixed for 24 h in a planetary ball mill (QM-3SP4, Nanjing University Instrument Plant, China), and then calcined for 24 h at 850, 1000 and 1100 °C. In each calcination step, the calcined powder was re-ground by ball milling for 24 h.

The textured ceramics were sintered by a two-step method using a SPS furnace (HPD 25/1 FCT, SPS furnace, Germany) [7,24]. In the first step, the powder was sintered in a graphite die (20 mm in diameter) under a pressure of 80 MPa at 1000 °C for 3 minutes. In the second step, the sintered ceramic was placed into a graphite die of 30 mm in diameter and then sintered again at 1050 °C for 5 min under a pressure of 80 MPa. During the second sintering stage, the grain growth rate along the *a*- and/or *b*-axis was faster than that along the *c*-axis, resulting in the grains with the *c*-axis aligned along the applied pressure direction. A heating rate of 100 °C/min was employed in both sintering steps. Finally, the SPS processed (denoted hereafter as SPSed) disks were annealed at 880 °C for 6 h in air to remove any residual carbon from the material. The colour of the annealed disk was light yellow with translucent feature. The density of the disks, as measured by the Archimedes method, was about 97.6±0.2%. For the microstructure observation and electrical property characterisation, the textured ceramics were cut perpendicular and parallel to the SPS pressing direction.

Crystal structure determination and refinements: The crystal structure of both the B2BT powder and the bulk ceramic sample were investigated by X-ray diffraction (XRD, Panalytical Xpert Pro diffractometer, Cu K_α radiation) at room temperature. The B2BT powder was

obtained from the SPSed disk by grounding. The Rietveld analysis on the room-temperature XRD data from the B2BT powder was performed using a GSAS software [26].

Microstructural characterisation: The microstructure of the textured ceramic samples was observed using a scanning electron microscope (SEM, FEI Inspect-F, Oxford). For SEM analysis, the ceramics were thermally etched at 1100 °C for 15 min. The average grain size was estimated from SEM images using the intercept line method [27].

Electrical property characterisation: An anisotropy in electrical properties of the SPSed samples was tested by applying an external electric field in the perpendicular [⊥] and parallel [//] direction to the SPS pressing direction. The temperature and frequency dependencies of the relative dielectric permittivity and loss tangent were measured by an LCR meter (Agilent, 4284A, USA) connected to a purpose-designed furnace and a low temperature test container. The polarisation-electric field (*P-E*) and current-electric field (*I-E*) loops were measured by a ferroelectric measurement instrument (NPL, UK). The testing frequency of a triangular voltage waveform for both the *P-E* and *I-E* loops was 10 Hz. The *P-E* and *I-E* loop measurement procedure involved the application of a triangular voltage waveform for the two fully completed cycles [7,25]. The piezoelectric constant, d_{33}, was measured using a Berlincourt piezo d_{33} meter (ZJ-3B, Institute of Acoustics, Chinese Academic of Science, Beijing).

Results and discussion

Fig. 1 shows the results of the Rietveld structure refinement for the B2BT powder using a mixed (*B2cb*+*I4*/*mmm*) model. The biphasic structural model considers the coexistence of the orthorhombic (SG: *B2cb*) and the tetragonal (SG: *I4*/*mmm*) phases in the material investigated.

The room-temperature XRD data were also analyzed by other structural models, as presented in Fig S1. The standard XRD diffraction data of the *I4/mmm* and *B2cb* phases were obtained from the reference JCPDS cards 01-073-6259 and 01-072-9952, respectively [16,18]. Table S1 summarizes the refined structural parameters for different structural models. A lower value of the weighted profile *R*-factor (R_{wp}) and the residual *R*-factor (R_p) in the mixed model, if compared to these obtained by the *B2cb* model and the *I4/mmm* model, suggests the coexistence of the two phases in B2BT ceramics. Moreover, the results of refinements indicate that the mass fraction of the orthorhombic structure and the tetragonal structure is about 72% and 28%, respectively. Hence, the main phase in B2BT ceramic is the polar *B2cb* phase.
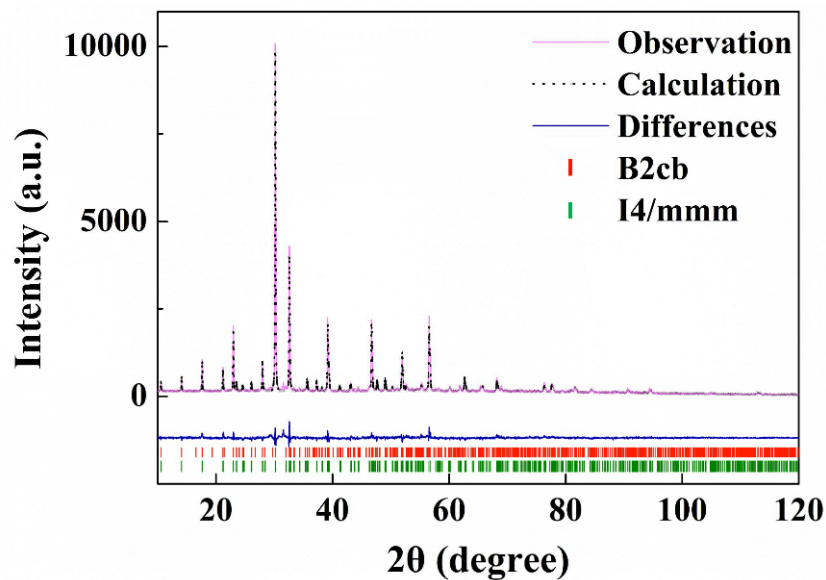

Figure 1. Rietveld XRD refinement of the B2BT powder using a mixed (*B2cb*+*I4*/*mmm*) model.

The XRD patterns of the SPSed B2BT ceramic collected at room temperature from the surface parallel and perpendicular to the SPS pressing direction are shown in Fig. 2. To quantify a preferred orientation, the XRD patterns were first indexed with reference to the orthorhombic *B2cb* crystal structure using the JCPDS card 01-072-9952. The XRD pattern from the surface perpendicular to the SPS pressing direction [Fig. 2(b)] shows strong (*00l*) diffraction peaks,

while the pattern from the surface parallel to the SPS pressing direction [Fig. 2(a)] has weak (*00l*) reflections. This behaviour implies that the SPSed samples are textured materials. The degree of texture was estimated using the Lotgering factor *f*, which can be expressed as follows [28]:

$$f = (p - p_o)/(1 - p_o) \tag{1}$$

where $p = \sum_l I(00l) / \sum_{hkl} I(hkl)$. $\sum_l I(00l)$ and $\sum_{hkl} I(hkl)$ are the sums of the intensities of (00*l*) and (*hkl*) reflections, respectively, and p_0 represents the value of p for a randomly oriented microstructure (in this study, p_0 is calculated from the XRD pattern of the powder ground from the SPSed ceramics). For the textured B2BT, the calculated *f*-factor is 0.62.
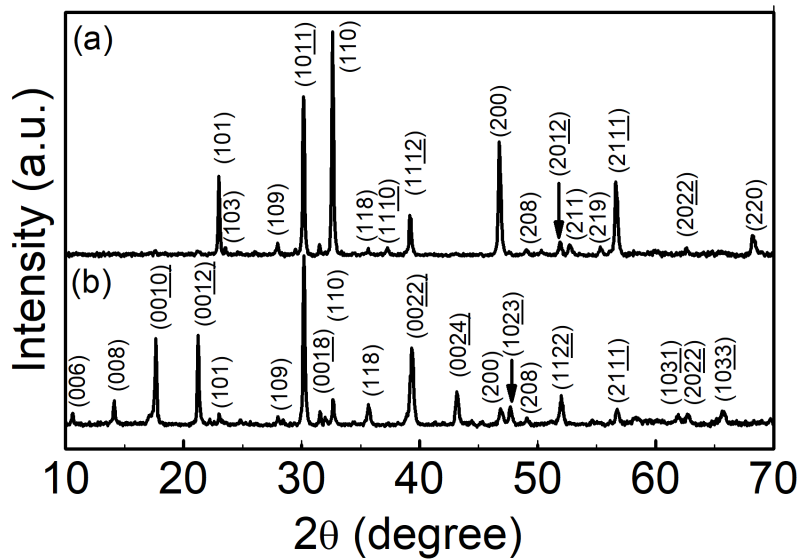

Figure 2. XRD patterns of the B2BT ceramic indexed by the *B2cb* space group. (a) data from the surface parallel, and (b) perpendicular to the SPS pressing direction.

Fig. 3 shows the SEM image of the polished, thermally etched sample with surface oriented parallel to the SPS pressing direction. The plate-like grains of B2BT form a brick-wall-like structure, in which the short axis is aligned preferentially parallel to the SPS pressing direction (marked by an arrow in Fig. 3). Thus, the grain morphology of the B2TB ceramics is consistent

9

with the preferred orientation identified by XRD (Fig. 2). The average length and thickness of plate-like grains are 2.0±0.5 μm and 0.5±0.2 μm, respectively. The calculated ferroelectric spontaneous polarisation P_s in each single grain along the length direction is 6.16±0.01 μC/cm^2 (in Fig. S2).
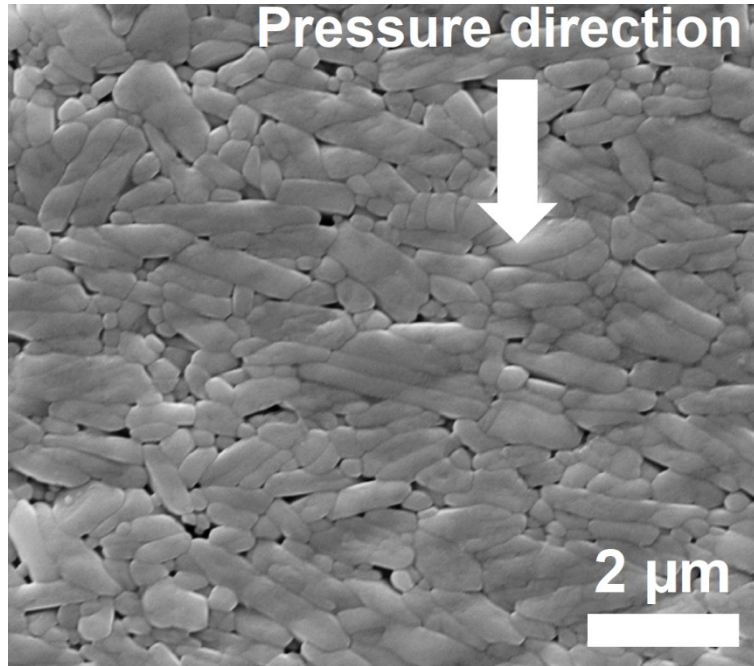

Figure 3. SEM image of the B2BT ceramic surface oriented parallel [∥] to the SPS pressing direction.

Fig. 4 and 5 display the relative dielectric permittivity (ε') and loss tangent (*tan δ*) of the B2BT ceramics measured at various frequencies (from 1 KHz to 1 MHz) along the different orientations as a function of the temperature. The temperature region in Fig. 4 and 5 is 25 °C ~ 600 °C, and -95 °C ~ 150 °C, respectively. For both [⊥] and [∥] directions, a very broad dielectric permittivity peak can be observed at around 240 °C and its position does not change with frequency. The temperature of the maximum of the relative dielectric permittivity is denoted as T_m. The value of T_m along [⊥] direction is close to that along [∥] direction. The peak value of relative dielectric permittivity at 10 kHz is about 1200 and 325 along [⊥] and [∥] directions, respectively. A diffuse phase transition has been observed in Ba-contained BLSFs

[12-14] and it can be attributed to the presence of cation disorder, where the Ba^{2+} ions enter the Bi_2O_2 layers, while Bi^{3+} are incorporated into the A-site of the perovskite units [15]. The frequency dependence of the loss tangent peak, a characteristic feature of RFEs with the cation disorder, is evident at low temperatures (Fig. 5).
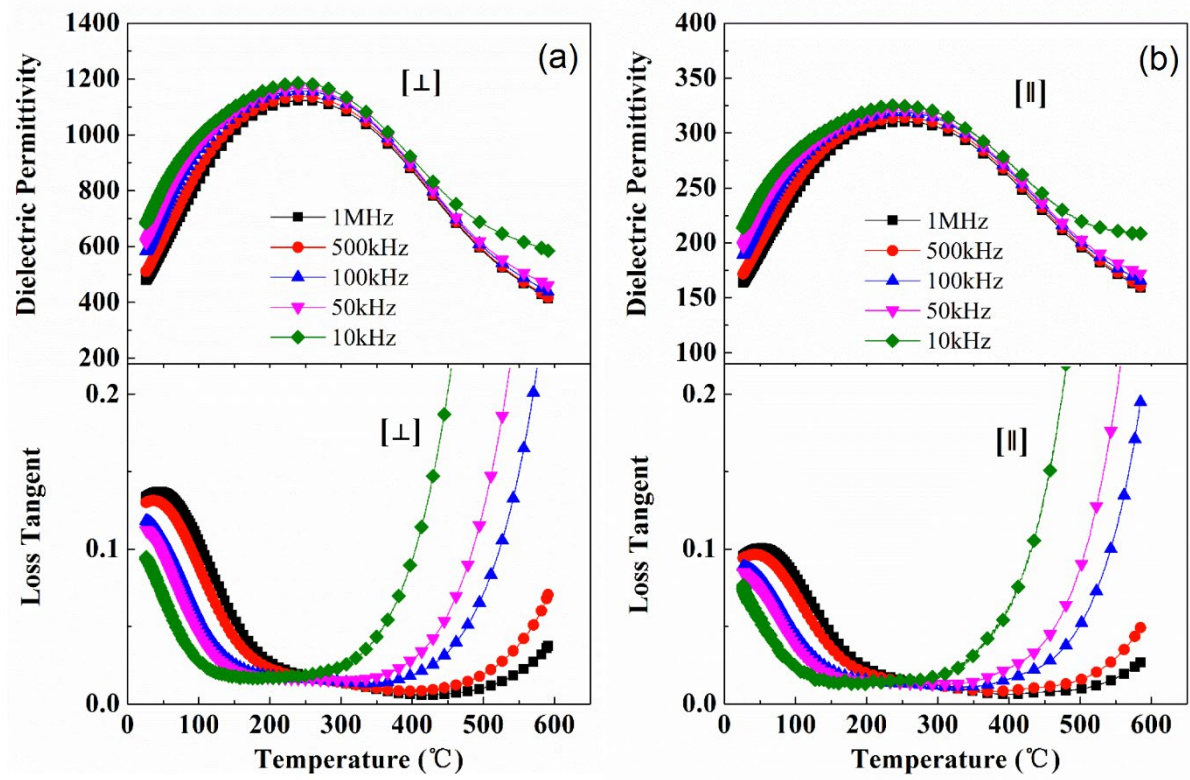

Figure 4. Temperature dependence of the relative dielectric permittivity and loss tangent: (a) along the direction [⊥], and (b) along the direction [∥] to the SPS pressing direction (measured from 25 °C to 600 °C).
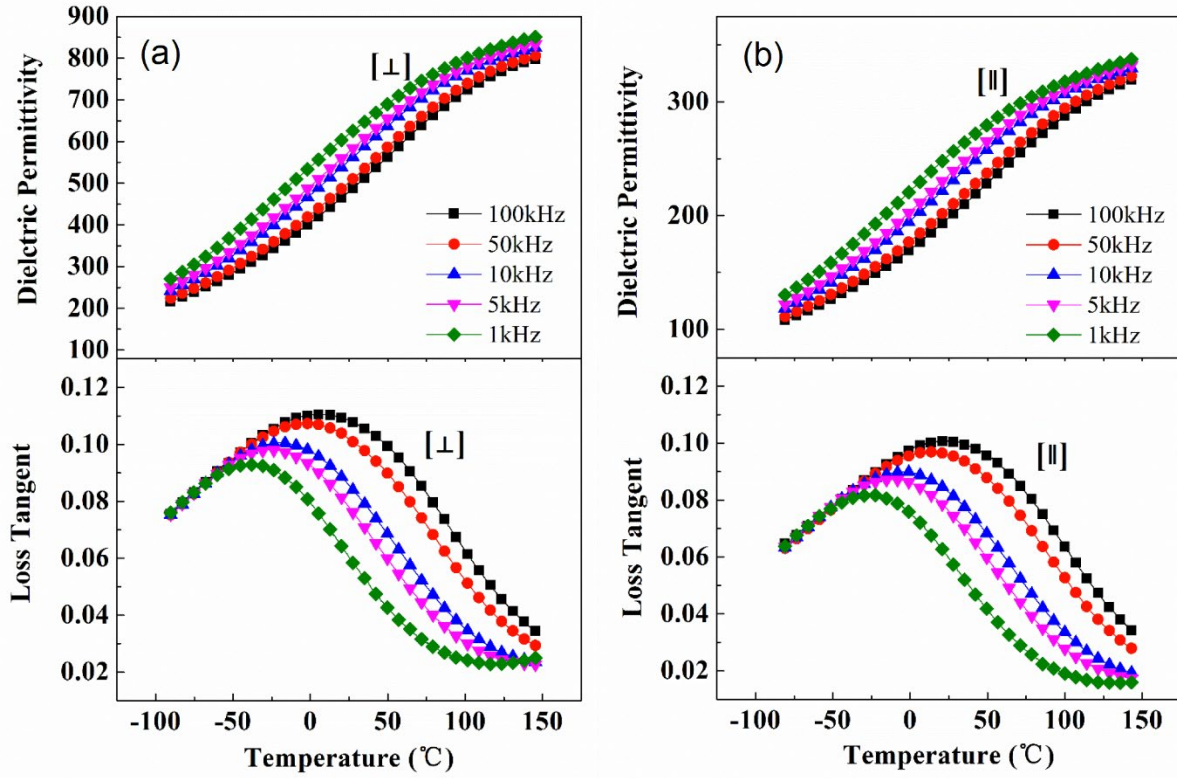
Figure 5. Temperature dependence of the relative dielectric permittivity and loss tangent: (a) along the direction [⊥], and (b) along the direction [∥] to the SPS pressing direction (measured from -95 °C to 150 °C).

To determine a degree of the dielectric relaxation, a modified Curie-Weiss law was employed [29,30]:

$$\frac{1}{\varepsilon} - \frac{1}{\varepsilon_m} = \frac{(T-T_m)^{\gamma}}{C_1} \tag{2}$$

where the degree of relaxation is described by the constant γ and C_1. The value of γ ranges between 1 and 2 (1 is for the conventional ferroelectrics and 2 is for an ideal relaxor) [30]. In this work, γ was determined from the dielectric permittivity data measured at 100 kHz in the temperature region of 240 °C - 600 °C (Fig. 4). The calculated value of γ is 1.35±0.05 and 1.23±0.05 in the perpendicular [⊥] and parallel [∥] direction to the direction of the SPS pressing,

respectively. The coinciding similarity of γ values has also been reported by Karthik *et al* in the textured $BaBi_2Nb_2O_9$ ceramics [31].

The dielectric relaxation of RFEs is known to follow the Vogel-Fulcher (V-F) law [12]:

$$f = f_0 exp[\frac{-E_a}{k_B(T_{m'}-T_{VF})}] \qquad (3)$$

where f is the experimental frequency, f_0 is the pre-exponential factor, E_a is the activation energy barrier between two equivalent polarisation states, k_B is the Boltzmann constant, $T_{m'}$ is the temperature corresponding to the loss tangent maxima, T_{VF} is the static dipolar freezing temperature, at which freezing of the dynamics of polar nanoregions occurs and the distribution of relaxation time becomes infinitely broad. By fitting the loss tangent behaviour in the temperature range of -95 °C – 150 °C, the relaxation V-F parameters were obtained (Table 1). T_{VF} of the B2BT ceramics along [∥] and [⊥] directions is 186 ± 6 K and 205 ± 18 K, respectively. From Table 1 one can see that the calculated values of both T_{vf} and E_a along [⊥] and [∥] directions are close to each other, which implies that the different dielectric behavior in the different directions can be linked with the same electrical dipoles.

Table 1. The fitting results of the textured B2BT ceramic by the Vogel-Fulcher law.

Direction	Freezing temperature, T_{VF} (K)	Activation energy, E_a (eV)	Pre-exponential factor, f_0 (Hz)
[⊥]	186 (±6)	0.102 (±0.012)	1.0×10^9
[∥]	205 (±18)	0.082 (±0.024)	1.5×10^7

The *P-E* and *I-E* curves of the B2BT ceramics tested along [⊥] and [∥] directions at a frequency of 10 Hz and room temperature are shown in Fig. 6. The maximum applied field for the *P-E* loop measurement in the perpendicular [⊥] and parallel [∥] directions was 120 kV/cm and 110 kV/cm, respectively. The appearance of slim *P-E* loops supports our previous conclusions about the relaxor behaviour of B2BT ceramics. The recoverable energy density, *J*, can be calculated by integrating the *P-E* loops according to the following equation [2]:

$$J = \int_{P_r}^{P_s} E dP \qquad (4)$$

where *E* is the applied electric field, P_r is the remanent polarisation and P_s is the saturated polarisation. The calculated recoverable energy density along [⊥] and [∥] directions is 0.41 ± 0.01 J/cm^3 and 0.14 ± 0.01 J/cm^3, respectively. The value in the perpendicular direction is close to the recoverable energy density of relaxor $Pb(Mg_{1/3}Nb_{2/3})O_3$ based ceramics (0.47 J/cm^3) [2], which are currently used as capacitors for high power energy storage. This makes the B2BT ceramics with high T_m a suitable candidate for replacement of $Pb(Mg_{1/3}Nb_{2/3})O_3$-derived capacitors in energy storage applications, where elevated temperatures appear during operation.

It is well known that ferroelectric domain switching in an ordinary ferroelectric is manifested by sharp switching current peaks in the 1st and the 3rd quadrants of the *I-E* loop [32,33]. In Fig. 6, these peaks are marked as P1 and P3. Interestingly, the *I-E* loops of the B2BT ceramic display additional peaks, P2 and P4, which appear in the 2nd and the 4th quadrant of the *I-E* loop in course of decreasing electric field. Although the P2 and P4 peaks in the B2BT [∥] sample are not as obvious as these of the [⊥] sample, they are discernible in the *I-E* loops of both samples, as shown in Fig. 6(b). Similar observations were previously reported for $Bi_{0.5}Na_{0.5}TiO_3$-based ferroelectric materials and the appearance of four switching current peaks in the *I-E* loop was linked with electric field-induced reversible transitions [34-36]. However,

this is the first time, to our best knowledge, that four switching current peaks are observed in the *I-E* loops of the BLSFs family.
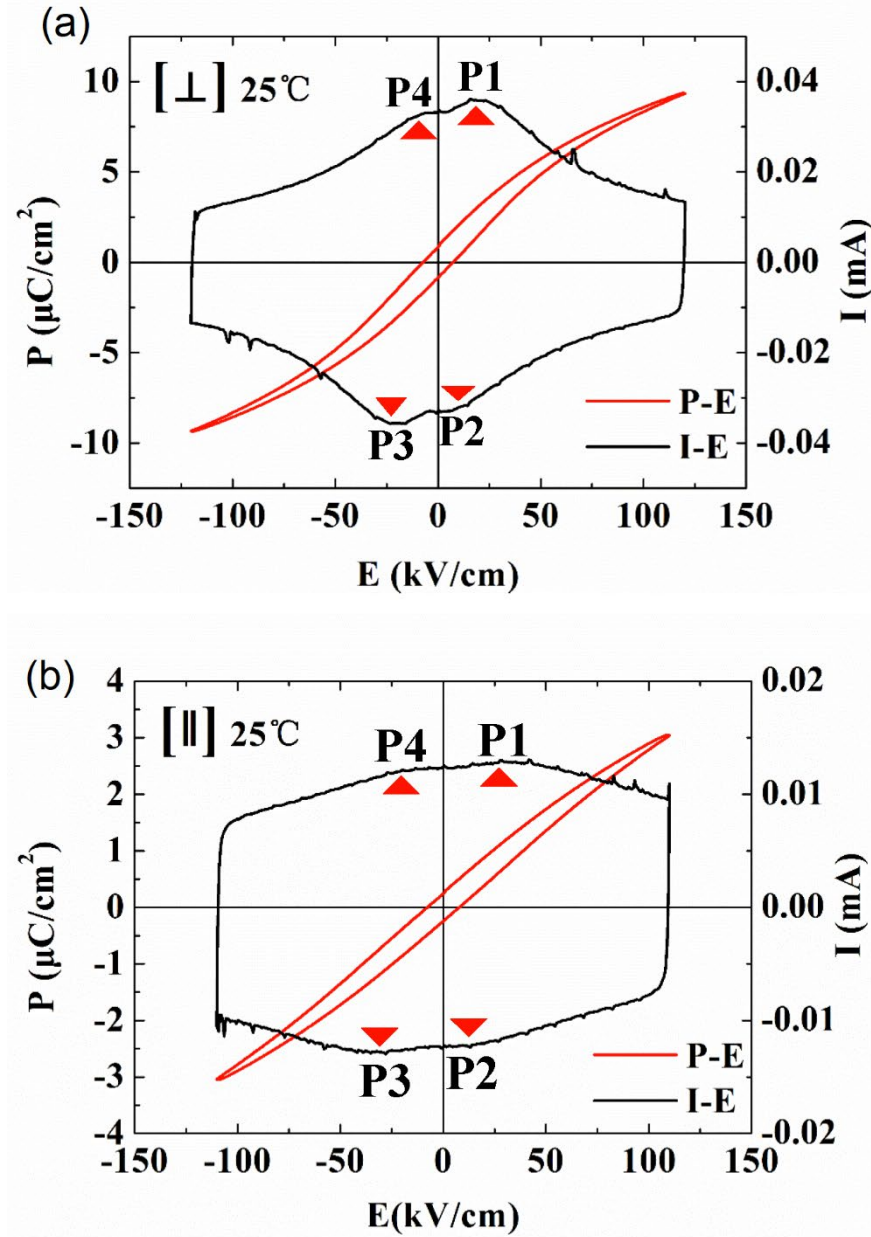

Figure 6. *P-E* and *I-E* loops of the B2BT ceramics measured (a) along the direction [⊥], and (b) along the direction [∥] to the SPS pressing direction (25 °C). The calculated recoverable energy density along the [⊥] and [∥] directions is 0.47 ± 0.01 J/cm^3 and 0.14 ± 0.01 J/cm^3, respectively.

Figs. 7 illustrates the evolution of the *P-E* and *I-E* loops of the B2BT [⊥] ceramics with increasing temperature from 25 °C to 225 °C. The *P-E* and *I-E* loops of the B2BT [∥] ceramics as a function of temperature are shown in Fig. 8 and Fig. S3. The four switching current peaks (P1, P2, P3 and P4) are clearly visible in the *I-E* loop of both the [⊥] and [∥] ceramic samples in the temperature region from 25 °C up to 100 °C. While the switching current peaks P1 and P3 are discernible up to 225 °C for both the [⊥] and [∥] ceramics, the P2 and P4 peaks disappear at temperatures above 100 °C. The *P-E* loops are slim over the all temperature range studied. The remanent polarisation (P_r) of both the B2BT [⊥] and [∥] ceramics slightly increases with the increasing temperature. Such an enhancement of the polarisation can be attributed to a temperature-driven increase in leakage current [32,33].
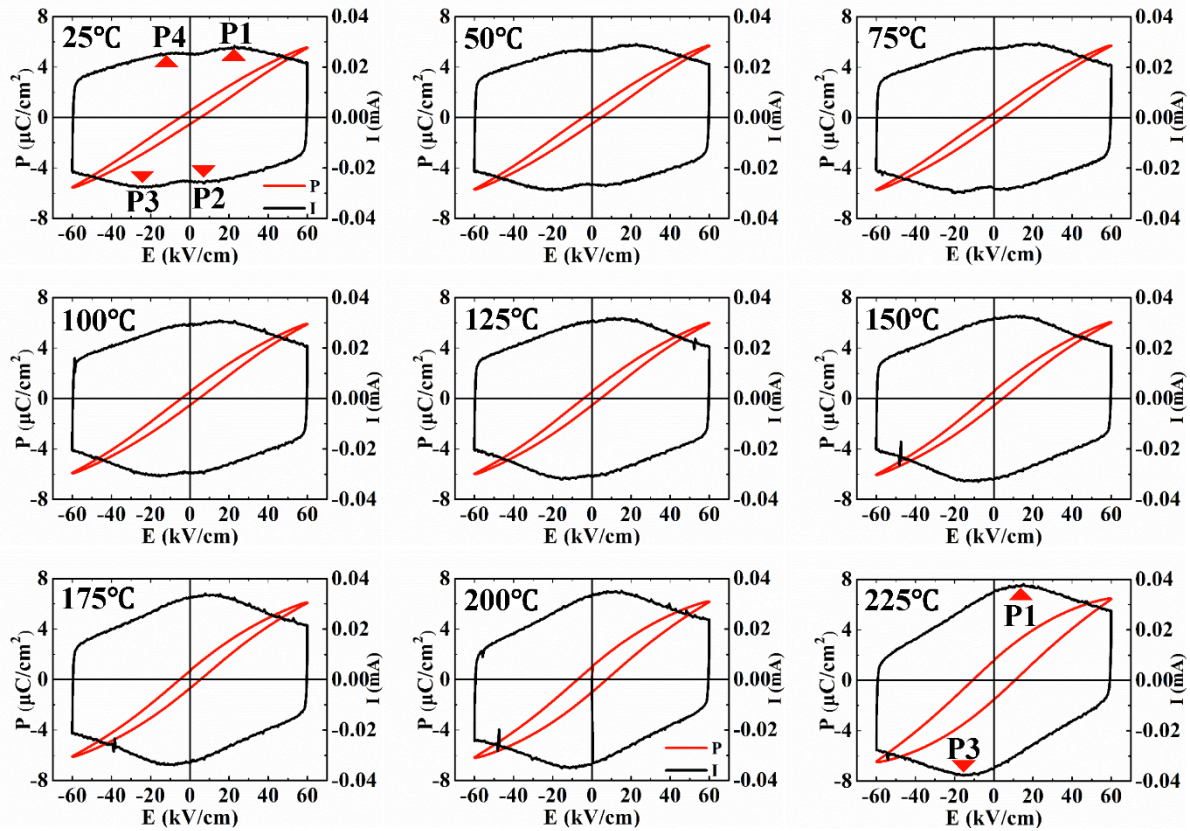

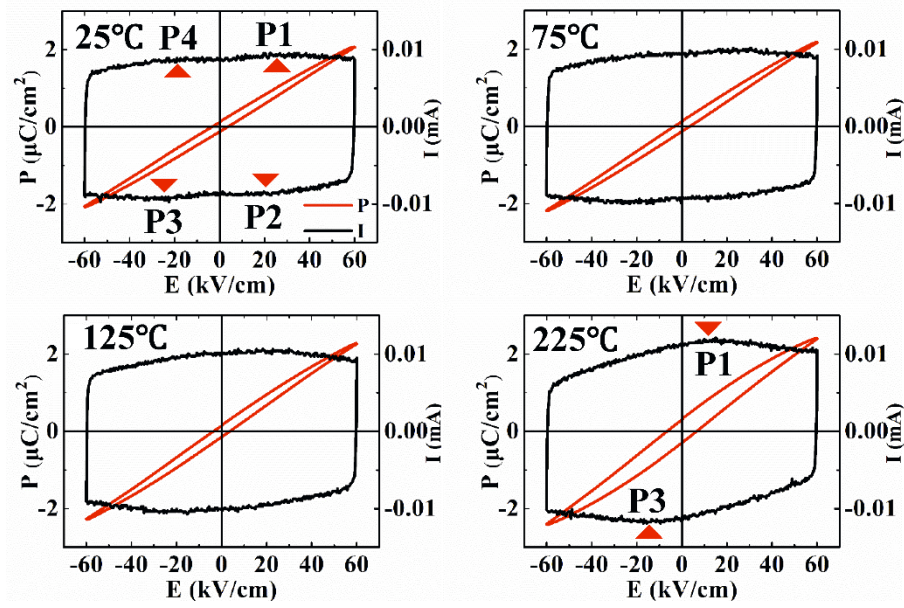Figure 7. *P-E* and *I-E* loops of the B2BT ceramics measured along the [⊥] direction at different temperatures from 25 °C to 225 °C.

Figure 8. *P-E* and *I-E* loops of B2BT ceramics measured along the [∥] direction at different temperatures from 25 °C to 225 °C.

As shown in Fig. 6(a), the field induced polarisation (9.0 µC/cm^2) is relatively high, while the remnant polarisation (P_r = 0.82 µC/cm^2) is extremely low, which indicates that the electric field-induced polarisation is unstable when the applied field is removed. The piezoelectric constant d_{33} of the poled B2BT [⊥] ceramics is 0.4±0.1 pC/N, whereas there was no detecable pizeoelectric response from the [∥] sample. Although, the measured d_{33} value of [⊥] ceramics is very small, it is far beyond the instrumental error of the piezo d_{33} meter (±0.1 pC/N). Thus, we propose that the textured B2BT ceramics exhibits the piezoelectric response in the direction perpendicular to the direction of the SPS pressing. The weak piezoelectricity is consistent with the extremely small value of P_r [Fig. 6(a)]. The anisotropic behaviour of d_{33} was also observed in other textured BLSF ceramics [7,24]. From our ferroelectric and piezoelectric property studies, we can conclude that the B2BT ceramic is a relaxor ferroelectric.

Most ferroelectric materials undergo a structural phase transition from a high-temperature paraelectric phase into a low-temperature ferroelectric phase at the so-called Curie point (T_c). The B2BT ceramic at room temperature consists of the ferroelectric *B2cb* phase, which is the dominant phase, and the minor paraelectric *I4/mmm* phase. This suggests that the high-temperature paraelectric phase does not fully transform into the ferroelectric phase on cooling. We believe that the evolution of the four switching current peaks in the *I-E* loops (Figs. 6-8) can be related to the structure evolution and the temperature dependent polarisation reversal in B2BT. The ferroelectric orthorhombic phase is thermally stable up to T_m or T_c (~ 240 ºC). The application of a sufficiently high electric field to a ferroelectric may induce an irreversible transition from random orientated small domains into strongly aligned large domains via domain switching [32]. The majority of the aligned domains in the B2BT ceramics does not backswitch upon removal or reduction of the electric field in the temperature range from 25 ºC to 225 ºC. This behaviour results in the appearance of the P1 and P3 peaks in the *I-E* loop. However, when the paraelectric tetragonal phase is cooled down from the so-called Burns temperature T_B (normally higher than T_m or T_c), a localized symmetry breaking (i.e. short-range order) may occur [37]. As a consequence, weak polar nanoregions (PNRs) are formed within the non-polar paraelectric phase, giving rise to the onset of relaxor characteristics of the tetragonal *I4*/*mmm* phase. The relaxor phase is subject of strong thermal fluctuations, and thus it is the thermally unstable structure. Upon further cooling, a glass-like transition occurs at the freezing temperature T_{VF} (~ 200 K, see Table 1), where the thermal fluctuations of PNRs vanish. At temperatures above T_{VF}, a reversible electric field-induced transition may occur in the relaxor phase. The application of an external electric field enables the weak polar state to transform into a long-range ordered ferroelectric state, which contributes to the electrical polarisation and switching current peaks at the 1st and 3rd quadrant of the *I-E* loops (Figs. 6-8). However, this electric field-induced polar state is highly unstable and returns back to its initial

18

state immediately upon removal or reduction of the electric field [35,36]. The recovering of the weak polar state is manifested in our relaxor system by the switching current peaks P2 and P4 in the *I-E* loops (Figs. 6-8). When the temperature is below 100 °C, both the electric field-induced transition in the paraelectric (or relaxor) phase and the ferroelectric domain switching in the ferroelectric phase can contribute to the switching current peaks P1 and P3 in the 1st and 3rd quadrant of the *I-E* loop. The switching current peaks P2 and P4 in the 2nd and 4th quadrant are only associated with the electric field-driven reversible transformation in the paraelectric (or relaxor) phase. When the temperature is above 100 °C, the electric field-induced transition is difficult to occur within the paraelectric (or relaxor) phase due to strong thermal fluctuations. Therefore, the P2 and P4 peaks are very small at temperatures above 100 °C (Figs. 7 and 8). The switching current peaks P1 and P3 are believed to be brought by the electric field-induced irreversible transition in the ferroelectric *B2cb* phase. The non-zero d_{33} value of the poled B2BT [⊥] ceramics is also supportive of the domain switching in the orthorhombic *B2cb* phase.

Conclusion

The highly textured B2BT ceramic was successfully prepared by SPS. Rietveld refinement of the room-temperature XRD data revealed that the crystal structure of the ceramic consists of both the polar orthorhombic (*B2cb*) phase and the non-polar tetragonal (*I4/mmm*) phase. A diffused phase transition at around 240 °C was identified in the sample measured along the perpendicular [⊥] as well as the parallel [∥] direction to the SPS pressing direction. No shift of the transition temperature with frequency was observed. Below 100 °C, four distinct switching current peaks were found in the *I-E* loops for both the [⊥] and [∥] samples. The evolution of the switching current peaks with increasing temperature is explained by the structural changes and temperature dependent polarisation reversal. In the temperature range from 25 °C to 225 °C,

the electric field-induced domain switching in the ferroelectric *B2cb* phase contributes to the switching current peaks only in the 1st and 3rd quadrant of the *I-E* loop. On the other hand, at temperatures between 25 °C and 100 °C, the electric field-induced reversible transition from a weak polar state to a long-range ordered ferroelectric state in the paraelectric (or relaxor) phase contributes to the switching current peaks at every quadrants of the *I-E* loop. Above 100 °C, no polarisation reversal within the paraelectric (or relaxor) phase was observed due to large thermal fluctuations. The observation of slim ferroelectric *P-E* hysteresis loops, the appearance of additional switching current peaks in the *I-E* loop and non-zero d_{33} piezoelectric coefficient (~ 0.4±0.1 pC/N for the B2BT [⊥] ceramic) are considered as a strong evidence of relaxor ferroelectric state in the samples investigated. The recoverable energy density of B2BT [⊥] ceramic is 0.41±0.01 J/cm^3, which is close to that of Pb(Mg$_{1/3}$Nb$_{2/3}$)O$_3$-based ceramics. Because of the excellent relaxor characteristics, B2BT ceramics with the preferred grain orientation is a potential candidate for high power energy storage.

Acknowledgments

References

1   Cowley, R. A., Gvasaliya, S. N., Lushnikov, S. G., Roessli, B. & Rotaru, G. M. Relaxing with relaxors: a review of relaxor ferroelectrics. *Advances in Physics* **60**, 229-327, doi:10.1080/00018732.2011.555385 (2011).

2   Zhang, T. F. *et al.* Energy-storage properties and high-temperature dielectric relaxation behaviors of relaxor ferroelectric $Pb(Mg_{1/3}Nb_{2/3})O_3$–$PbTiO_3$ ceramics. *Journal of Physics D, Applied Physics* **49**, 8, doi:DOI:101088/0022-3727/49/9/095302 (2016).

3   Koval, V., Alemany, C., Briančin, J. & Bruncková, H. Dielectric Properties and Phase Transition Behavior of xPMN-(1 − x)PZT Ceramic Systems. *Journal of Electroceramics* **10**, 19-29, doi:10.1023/A:1024023823871 (2003).

4   Koval, V. *et al.* Effect of PMN modification on structure and electrical response of xPMN–(1−x)PZT ceramic systems. *Journal of the European Ceramic Society* **23**, 1157-1166, doi:https://doi.org/10.1016/S0955-2219(02)00281-9 (2003).

5   Damjanovic, D. Materials for high temperature piezoelectric transducers. *Current Opinion in Solid State and Materials Science* **3**, 469-473, doi:https://doi.org/10.1016/S1359-0286(98)80009-0 (1998).

6   Turner, R. C., Fuierer, P. A., Newnham, R. E. & Shrout, T. R. Materials for high temperature acoustic and vibration sensors: A review. *Applied Acoustics* **41**, 299-324, doi:https://doi.org/10.1016/0003-682X(94)90091-4 (1994).

7   Yan, H. *et al.* A Lead-Free High-Curie-Point Ferroelectric Ceramic, $CaBi_2Nb_2O_9$. *Advanced Materials* **17**, 1261-1265, doi:10.1002/adma.200401860 (2005).

8   de Araujo, C. A. P., Cuchiaro, J. D., McMillan, L. D., Scott, M. C. & Scott, J. F. Fatigue-free ferroelectric capacitors with platinum electrodes. *Nature* **374**, 627, doi:10.1038/374627a0 (1995).

9   Park, B. H. *et al.* Lanthanum-substituted bismuth titanate for use in non-volatile memories. *Nature* **401**, 682, doi:10.1038/44352 (1999).

10   Irie, H., Miyayama, M. & Kudo, T. Structure dependence of ferroelectric properties of bismuth layer-structured ferroelectric single crystals. *Journal of Applied Physics* **90**, 4089-4094, doi:10.1063/1.1389476 (2001).

11   Irie, H., Miyayama, M. & Kudo, T. Electrical properties of a bismuth layer-structured $Ba_2Bi_4Ti_5O_{18}$ single crystal. *Journal of the American Ceramic Society* **83**, 2699-2704, doi:10.1111/j.1151-2916.2000.tb01619.x (2000).

12   Yan, H. *et al.* Orientation dependence of dielectric and relaxor behaviour in Aurivillius phase

BaBi$_2$Nb$_2$O$_9$ ceramics prepared by spark plasma sintering. *Journal of Materials Science:*

Materials in Electronics **17**, 657-661, doi:10.1007/s10854-006-0017-0 (2006).

13   Khokhar, A., Goyal, P. K., Thakur, O. P., Shukla, A. K. & Sreenivas, K. Influence of

lanthanum distribution on dielectric and ferroelectric properties of BaBi$_{4-x}$La$_x$Ti$_4$O$_{15}$ ceramics.

Materials Chemistry and Physics **152**, 13-25,

doi:https://doi.org/10.1016/j.matchemphys.2014.11.074 (2015).

14   Shimakawa, Y. *et al.* Crystal structures and ferroelectric properties of SrBi$_2$Ta$_2$O$_9$ and

Sr$_{0.8}$Bi$_{2.2}$Ta$_2$O$_9$. *Applied Physics Letters* **74**, 1904-1906, doi:10.1063/1.123708 (1999).

15   Tellier, J., Boullay, P., Manier, M. & Mercurio, D. A comparative study of the Aurivillius

phase ferroelectrics CaBi$_4$Ti$_4$O$_{15}$ and BaBi$_4$Ti$_4$O$_{15}$. *Journal of Solid State Chemistry* **177**,

1829-1837, doi:https://doi.org/10.1016/j.jssc.2004.01.008 (2004).

16   Aurivillius, B. F., P.H. Ferroelectricity in the compound Ba$_2$Bi$_4$Ti$_5$O$_{18}$. *Physical Review* **126**,

p893-p896, doi:10.1103/PhysRev.126.893 (1962).

17   Subbarao E, C. Crystal chemistry of mixed bismuth oxides with layer-type structure. *Journal*

of the American Ceramic Society **45**, 166-169, doi:10.1111/j.1151-2916.1962.tb11113.x

(2006).

18   Ismunandar *et al.* Structural studies of five layer Aurivillius oxides: A$_2$Bi$_4$Ti$_5$O$_{18}$ (A=Ca, Sr,

Ba and Pb). *Journal of Solid State Chemistry* **177**, 4188-4196,

doi:https://doi.org/10.1016/j.jssc.2004.07.032 (2004).

19   Lightfoot, P., Snedden, A., Blake, S. M. & Knight, K. S. Contrasting structural behavior in

the Aurivillius phase ferroelectrics Bi$_4$Ti$_3$O$_{12}$, BaBi$_4$Ti$_4$O$_{15}$ and Ba$_2$Bi$_4$Ti$_5$O$_{18}$. *MRS*

Proceedings **755**, DD4.7, doi:10.1557/PROC-755-DD4.7 (2011).

20   Fuentes, L. *et al.* Synchrotron radiation study of structural tendencies in Aurivillius Ceramics.

Ferroelectrics **339**, 209-218, doi:10.1080/00150190600740192 (2006).

21   Hou, R. Z. & Chen, X. M. Synthesis and dielectric properties of layer-structured compounds

A$_{n-3}$Bi$_4$Ti$_n$O$_{3n+3}$ (A = Ba, Sr, Ca) with n>4. *Journal of Materials Research* **20**, 2354-2359,

doi:10.1557/jmr.2005.0287 (2011).

22 Dubey, S. & Kurchania, R. Study of dielectric and ferroelectric properties of five-layer Aurivillius oxides: $A_2Bi_4Ti_5O_{18}$ (A = Ba, Pb and Sr) synthesized by solution combustion route. *Bulletin of Materials Science* **38**, 1881-1889, doi:10.1007/s12034-015-1043-4 (2015).

23 Park, S.-E. E. & Hackenberger, W. High performance single crystal piezoelectrics: applications and issues. *Current Opinion in Solid State and Materials Science* **6**, 11-18, doi:https://doi.org/10.1016/S1359-0286(02)00023-2 (2002).

24 Shen, Z. *et al.* Effective Grain Alignment in $Bi_4Ti_3O_{12}$ Ceramics by Superplastic-Deformation-Induced Directional Dynamic Ripening. *Advanced Materials* **17**, 676-680, doi:10.1002/adma.200401127 (2005).

25 Yan, H. X., Ning, H. P., Zhang, H. T. & Reece, M. J. Textured high Curie point piezoelectric ceramics prepared by spark plasma sintering. *Advances in Applied Ceramics* **109**, 139-142, doi:10.1179/174367509X12502621261334 (2010).

26 Larson, A. C. & Von Dreele, R. B. *Generalized Structure Analysis System (GSAS)*. Vol. 86-789 (2000).

27 Brandon, D. & Kaplan, W. *Microstructural Characterization of Materials, 2nd Edition*. (2008).

28 Takenaka, T. Grain Orientation and Electrical Properties of Hot-Forged $Bi_4Ti_3O_{12}$ Ceramics. *Japanese journal of applied physics* **19**, 31-39, doi:10.1143/JJAP.19.31 (1980).

29 Uchino, K. & Nomura, S. Critical exponents of the dielectric constants in diffused-phase-transition crystals. *Ferroelectrics* **44**, 55-61, doi:10.1080/00150198208260644 (1982).

30 Maiti, T., Guo, R. & Bhalla, A. S. Structure-property phase diagram of $BaZr_xTi_{1-x}O_3$ system. *Journal of the American Ceramic Society* **91**, 1769-1780, doi:10.1111/j.1551-2916.2008.02442.x (2008).

31 Karthik, C. & Varma, K. B. R. Dielectric and pyroelectric anisotropy in the melt-quenched barium bismuth niobate ceramics. *Journal of Electroceramics* **18**, 347-353, doi:10.1007/s10832-007-9186-3 (2007).

32   Jin, L., Li, F., Zhang, S. & Green, D. J. Decoding the fingerprint of ferroelectric loops: comprehension of the material properties and structures. *Journal of the American Ceramic Society* **97**, 1-27, doi:10.1111/jace.12773 (2013).

33   Yan, H. *et al.* The contribution of electrical conductivity, dielectric permittivity and domain switching in ferroelectric hysteresis loops. *Journal of Advanced Dielectrics* **01**, 107-118, doi:10.1142/S2010135X11000148 (2011).

34   Karthik, T., Radhakrishanan, D., Narayana, C. & Asthana, S. Nature of electric field driven ferroelectric phase transition in lead-free $Na_{1/2}Bi_{1/2}TiO_3$: In-situ temperature dependent ferroelectric hysteresis and Raman scattering studies. *Journal of Alloys and Compounds* **732**, 945-951, doi:https://doi.org/10.1016/j.jallcom.2017.10.126 (2018).

35   Dinh, T. H. *et al.* Nanoscale ferroelectric/relaxor composites: Origin of large strain in lead–free Bi–based incipient piezoelectric ceramics. *Journal of the European Ceramic Society* **36**, 3401-3407, doi:https://doi.org/10.1016/j.jeurceramsoc.2016.05.044 (2016).

36   Liu, L. *et al.* Large strain response based on relaxor-antiferroelectric coherence in $Bi_{0.5}Na_{0.5}TiO_3$–$SrTiO_3$–$(K_{0.5}Na_{0.5})NbO_3$ solid solutions. *Journal of Applied Physics* **116**, 184104, doi:10.1063/1.4901549 (2014).

37   Shvartsman, V. V. & Lupascu, D. C. Lead-Free Relaxor Ferroelectrics. *Journal of the American Ceramic Society* **95**, 1-26, doi:10.1111/j.1551-2916.2011.04952.x (2011).

Supplementary information

Crystal structure and electrical properties of textured Ba₂Bi₄Ti₅O₁₈ ceramics

Jun Cao,[1] Vladimir Koval,[2] Hangfeng Zhang,[1] Yunyin Lin,[1] Jiyue Wu,[1] Nan Meng,[1]

Yan Li,[4] Zheng Li,[1*] Hongtao Zhang,[3*] Haixue Yan[1]

[1] School of Engineering and Materials Science, Queen Mary University of London, Mile End Road, London, E1 4NS, United Kingdom

[2] Institute of Materials Research, Slovak Academy of Sciences, Watsonova 47, 04001 Kosice, Slovakia

[3] Department of Materials, Loughborough University, Leicestershire, LE11 3TU, United Kingdom

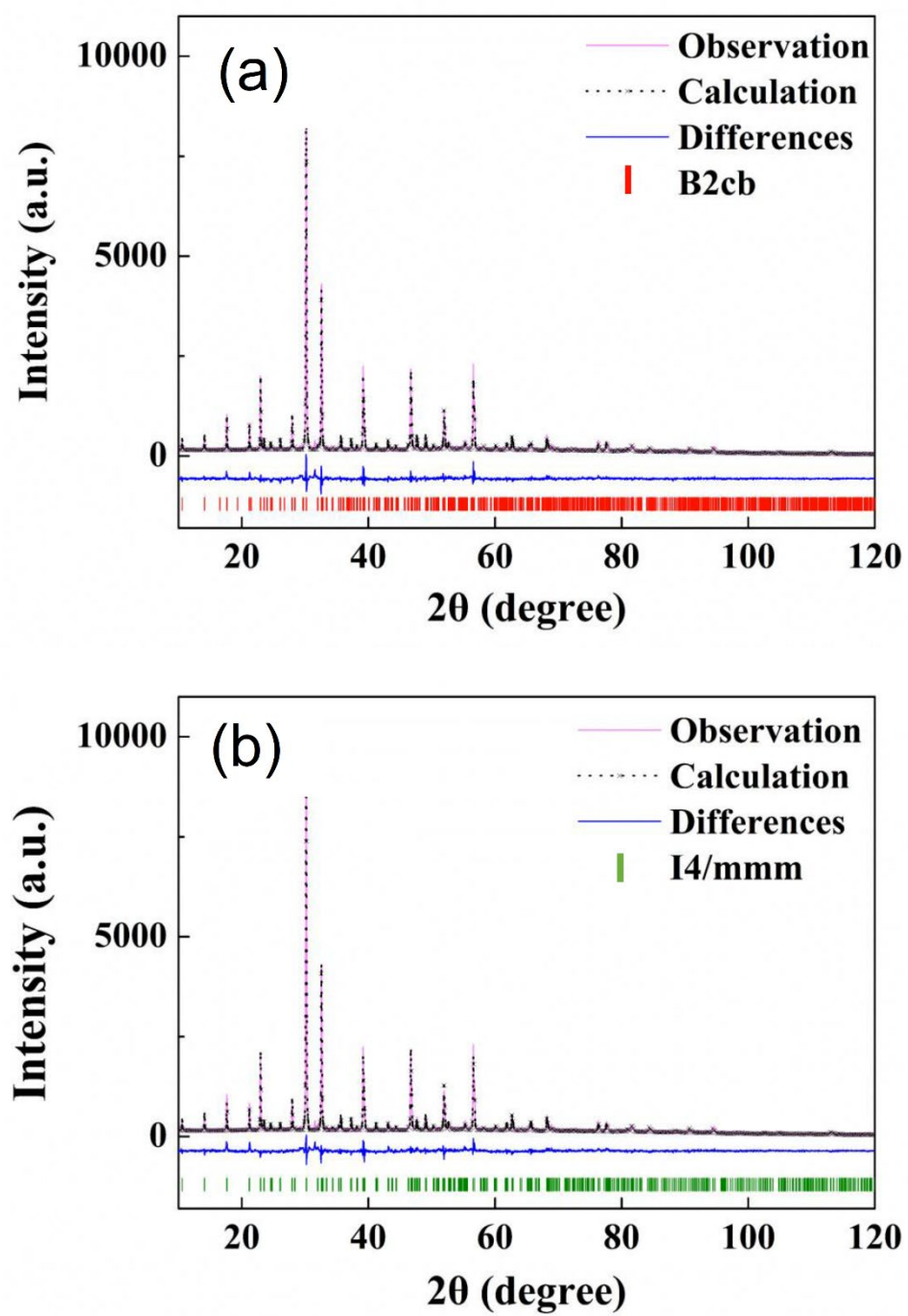[4] Gemmological Institute, China University of Geosciences, Wuhan, 430074, PR China

Figure S1. Rietveld analysis of the room-temperature XRD data collected for the B2BT powder. (a) the *B2cb* structural model, and (b) the *I4/mmm* model.

Table S1. The refined structural parameters for the B2BT powder, as obtained by the Rietveld method using different structural models.

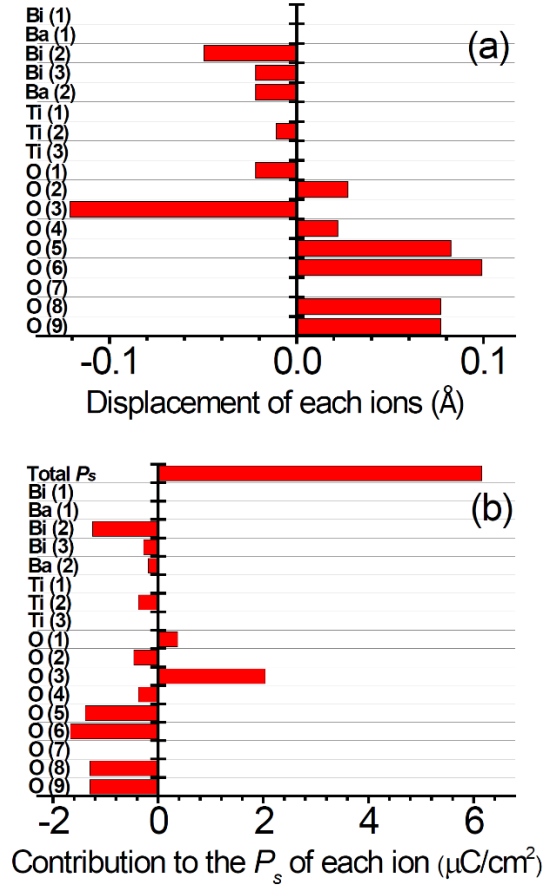| Phase existence state	Space group	Refined lattice parameters			wt (%)	Reliability factors		
		a (Å)	b (Å)	c (Å)		R_{wp}	R_p	x^2
Single phase	$B2cb$	5.5009(6)	5.4992(6)	50.379(2)	100	0.1122	0.0866	2.399
	$I4/mmm$	3.8892(1)	3.8892(1)	50.384(2)	100	0.1171	0.0854	2.615
Two phases	$B2cb$	5.5009(7)	5.4975(7)	50.417(4)	71.8	0.1080	0.0829	2.227
	$I4/mmm$	3.8904(7)	3.8904(7)	50.323(3)	28.2			

Figure S2. (a) Ionic displacements and (b) contributions of each constituent ion to the total spontaneous polarisation P_s of B2BT.

The co-operative displacement of the atoms from the corresponding positions in the parent tetragonal (*I4/mmm*) structure along the *a*-axis leads to the appearance of the ferroelectric spontaneous polarisation P_s in the B2BT ceramics. Fig. S2 shows the ionic displacements and their contribution to the total P_s. P_s is calculated as follows [1]:

$$P_s = \sum_i (m_i * \Delta x_i * Q_i e)/V \qquad (1)$$

where m_i is the site multiplicity, Δx_i is the absolute atomic displacement along the *a*-axis, $Q_i e$ is the ionic charge for the *i*th constituent ion, and V is the volume of the unit cell. The atomic displacement data for the non-polar structure (*I4/mmm*) and the polar *B2cb* structure were obtained from the reference database files JCPDS-01-073-6259 and JCPDS-01-072-9952,

respectively [2,3]. The calculated P_s is 6.16 μC/cm^2, which is smaller than that of a single

crystal (P_s = 12 μC/cm^2) [4,5]. The difference in polarisation can be attributed to the increased
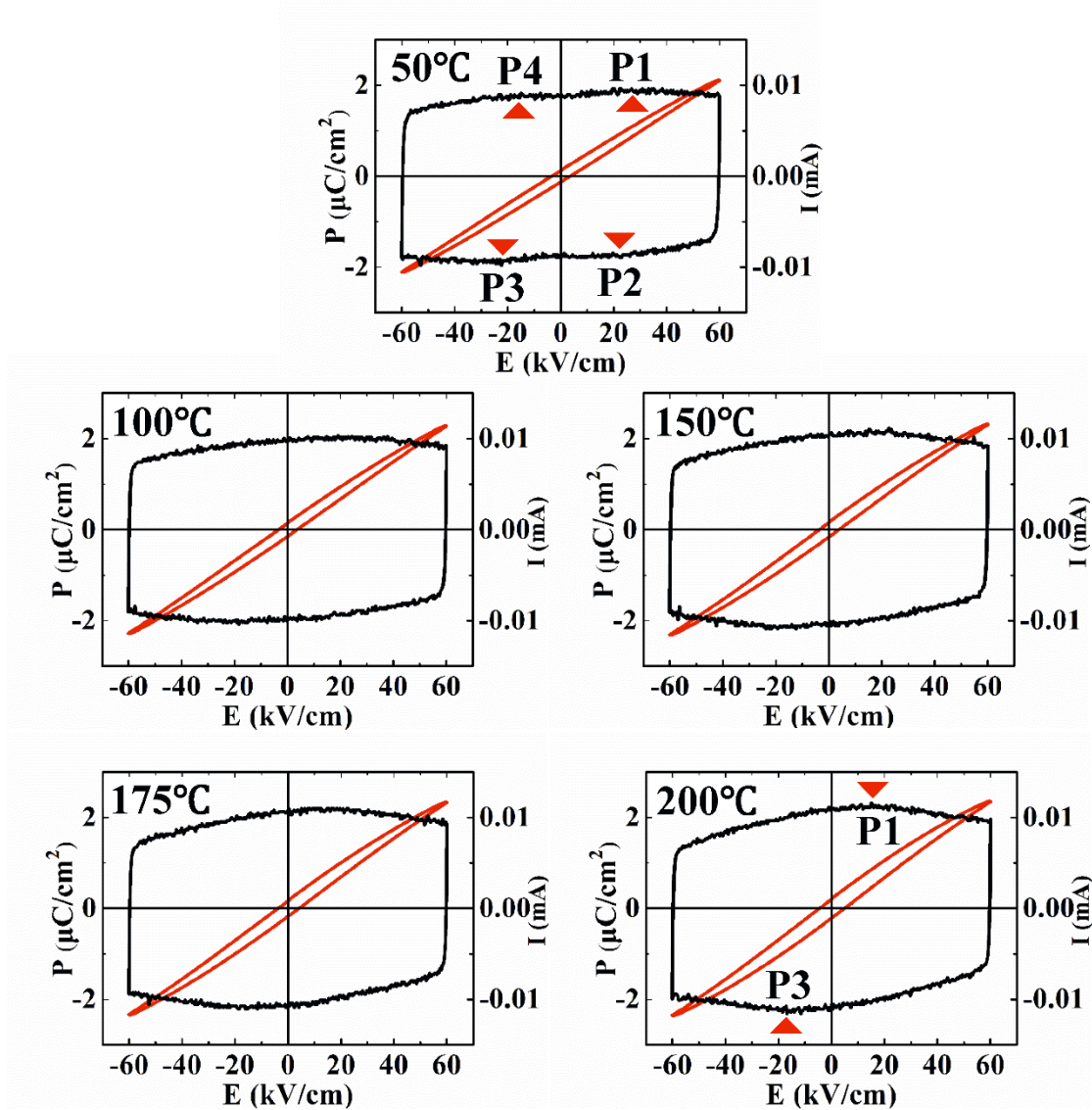
electrical conductivity of the B2BT single crystal [6].

Fig. S3 *P-E* and *I-E* loops of the B2BT ceramic measured along the [∥] direction at five

different temperatures

References

1. Shimakawa, Y. *et al.* Crystal structures and ferroelectric properties of $SrBi_2Ta_2O_9$ and $Sr_{0.8}Bi_{2.2}Ta_2O_9$. *Applied Physics Letters* **74**, 1904-1906, doi:10.1063/1.123708 (1999).

2. Aurivillius, B. F., P.H. Ferroelectricity in the compound $Ba_2Bi_4Ti_5O_{18}$. *Physical Review* **126**, p893-p896, doi:10.1103/PhysRev.126.893 (1962).

3. Ismunandar *et al.* Structural studies of five layer Aurivillius oxides: $A_2Bi_4Ti_5O_{18}$ (A=Ca, Sr, Ba and Pb). *Journal of Solid State Chemistry* **177**, 4188-4196, doi:https://doi.org/10.1016/j.jssc.2004.07.032 (2004).

4. Irie, H., Miyayama, M. & Kudo, T. Structure dependence of ferroelectric properties of bismuth layer-structured ferroelectric single crystals. *Journal of Applied Physics* **90**, 4089-4094, doi:10.1063/1.1389476 (2001).

5. Irie, H., Miyayama, M. & Kudo, T. Electrical properties of a bismuth layer-structured $Ba_2Bi_4Ti_5O_{18}$ single crystal. *Journal of the American Ceramic Society* **83**, 2699-2704, doi:10.1111/j.1151-2916.2000.tb01619.x (2000).

6. Yan, H. *et al.* The contribution of electrical conductivity, dielectric permittivity and domain switching in ferroelectric hysteresis loops. *Journal of Advanced Dielectrics* **01**, 107-118, doi:10.1142/S2010135X11000148 (2011).